Proceedings of the Institute of Acoustics

THE EFFECT OF GRATING LOBES IN SYNTHETIC APERTURE SONAR IMAGING

M. Opperud Department of Informatics, University of Oslo, Oslo, Norway
A. Austeng Department of Informatics, University of Oslo, Oslo, Norway
R. E. Hansen Norwegian Defence Research Establishment (FFI), Kjeller, Norway
M. Geilhufe Norwegian Defence Research Establishment (FFI), Kjeller, Norway

1 INTRODUCTION

Synthetic aperture sonar (SAS) synthesizes a long array by coherently combining consecutive pulses, which consequently improves the along-track resolution[1]. The SAS system also improves the area coverage rate by using a single transmitter and multiple receivers. By controlling the pulse repetition frequency relative to the platform speed, the resulting long array is well sampled without grating lobe artifacts according to the phase center approximation[2]. However, grating lobe-like errors can occur because of deviations from a straight line, crab, errors in the navigational solution, or inaccuracies in the calculated scene geometry[3,4]. This error appears as defocused periodic replicas of real targets in the image and is a common type of degradation in SAS images[5]. We term this periodic error (PE) grating lobes to avoid confusion with grating lobes due to undersampling. By characterizing and estimating them, it can be measured how much an image is degraded and the errors can potentially be removed.

We suggest using the Aperture Smoothing Function (ASF), a concept from array signal processing[6], to characterize the PE grating lobes. The characteristics we want to describe are the position, spread, and amplitude of the PE grating lobes. The standard ASF is only valid for far-field and single frequency operation. Since SAS systems transmits unfocused pulses with a large bandwidth, we expand the single frequency ASF to a broadband ASF by summing the single frequency ASF for all frequencies in the pulse.

We test our approach on real data collected by a HUGIN autonomous underwater vehicle (AUV) carrying a HISAS interferometric SAS and on datasets generated from a point scatterer-simulator in the FOCUS SAS Processing Toolbox, developed by FFI[7]. The real data and point scatterer dataset are induced by realistic navigation errors[5]. We also describe other effects of the PE grating lobes in the data, such as the near field, range spread, and rotation that is not described by the ASF. We show results using theory, simulations, and how the periodic error grating lobes occur in SAS images.

This paper is based on the master's thesis work by Opperud[8].

2 PERIODIC ERROR GRATING LOBES

One of the reasons why PE grating lobes occur in SAS images is because of inaccurate navigation[3]. The three angles of freedom that can be inaccurately estimated are yaw, pitch, and roll. Inaccurate estimation of yaw or pitch leads to time delay errors in the beamformer that coherently combines the received data. Consequently, for multi-element receiver SAS systems, the time delay errors form a periodic sawtooth pattern in the synthetic aperture. An illustration of inaccurately estimated yaw is shown in Figure 1. Other ways of getting sawtooth phase errors in the beamformer are by imaging plane errors in combination with an out-of-plane deviation[3,4]. It has been shown that the PE grating lobes can be derived from the Fourier series of a sawtooth phase error function[9]. We consider the yaw error and derive the PE grating lobes using the ASF.

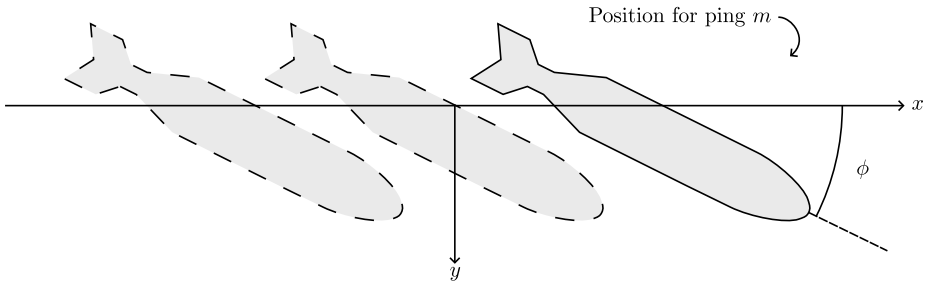

Figure 1: Sonar vehicle with a yaw error ϕ. The z axis points inwards. For illustrative purposes the distance between every ping is exaggerated. Retrieved from[8].

The ASF[6] describes an array's spatial response as a function of the incoming wave's wavevector $\vec{k}$. For a linear array with M transducers, the ASF is given by

$$W_a(\vec{k}) = \sum_{m=0}^{M-1} W_{El,m}(\vec{k}) w_m e^{j\vec{k}\cdot\vec{r}_m}, \tag{1}$$

where $\vec{r}_m$ are transducer positions, w_m are the transducer weights, and $W_{El,m}(\vec{k})$ are the element responses. The wavevector $\vec{k}$ is the vector pointing in the direction of wave propagation. Assume a two-dimensional Cartesian coordinate system with a uniform linear array placed along the x-axis and the array normal points along the y-axis, the wavevector is given as $\vec{k} = [k_x, k_y] = k[\sin\theta, \cos\theta]$ where θ is the incidence angle measured from the array normal. The magnitude of the wavevector is the spatial frequency $k = \frac{2\pi}{\lambda}$ where λ is the wavelength. Note that Equation (1) is only valid in the far field for a single frequency.

The total ASF of a system consisting of a set of transmitters and receivers is given as the product of the two. We assume a SAS system moving at a straight line and having M transmits at positions mL_{tx} and receiving on an N element array with interelement distance D_{Rx}. The corresponding total ASF becomes

$$W_{tot}(k_x) = W_{El,tx}(k_x) W_{El,rx}(k_x) W_{Tx}(k_x) W_{Rx}(k_x), \tag{2}$$

where the transmit and receive beampatterns are given by

$$W_{Tx}(k_x) = \sum_{m=1}^{M} w_m e^{jk_x 2L_{Tx} m} \quad \text{and} \quad W_{Rx}(k_x) = \sum_{n=1}^{N} w_n e^{jk_x D_{Rx} n}. \tag{3}$$

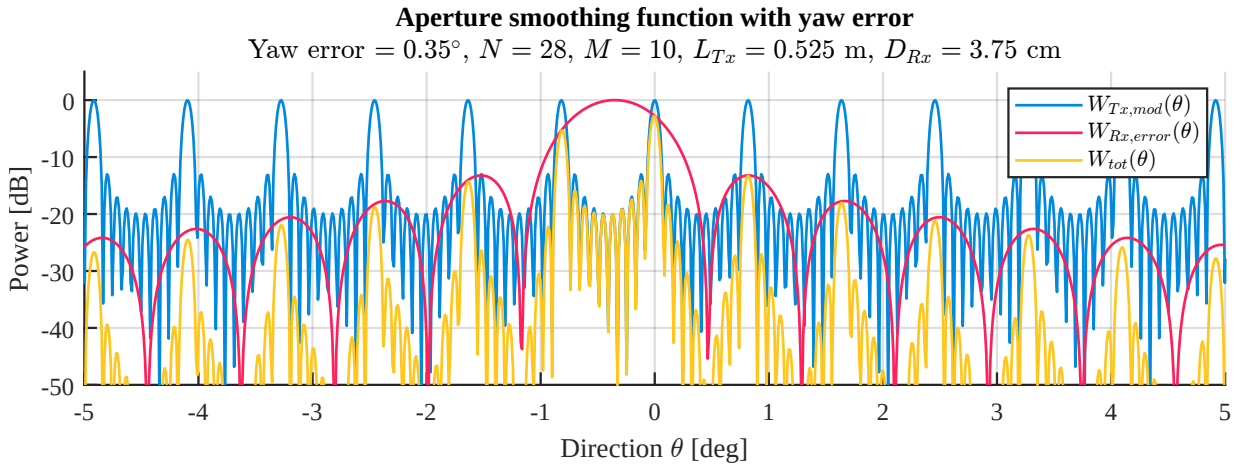

Figure 2: The single frequency ASF of a SAS vehicle with a yaw error of $\theta^\circ = 0.35^\circ$***. The receivers and transmitters are uniformly weighted.*** $W_{Rx,error}(\theta)$ ***is the receiver beampattern with a yaw error*** $W_{Rx}(\theta - \theta^\circ)$***. Retrieved from[8].***

$W_{El,tx}(k_x)$ and $W_{El,rx}(k_x)$ are the element responses of the transmitter and receivers respectively.

We include the time delay errors due to yaw error in the ASF by steering the receive beampattern in a direction opposite to the yaw error, $k_x^\circ = k \sin\theta^\circ$. Thus, the ASF for a SAS system with a yaw error is given as

$$W_{tot,error}(k_x) = W_{El,tx}(k_x) W_{El,rx}(k_x) W_{Tx}(k_x) W_{Rx}(k_x - k_x^\circ). \tag{4}$$

The ASF product in Equation (4) for a yaw error of $\theta^\circ = 0.35^\circ$ is shown in Figure 2. There are unequally weighted grating lobes because the receiver beampattern no longer cancels the grating lobes from the transmit beampattern. These asymmetrical grating lobes correspond to the PE grating lobes and are placed at multiples p of the angles

$$u = \sin\theta = \frac{\lambda}{2L_{Tx}} p. \tag{5}$$

This corresponds to the angles derived by Cook and Brown[9].

The total field at a point in front of a transducer, is a sum of each contribution from each frequency component in the signal[10]. We extend the ASF model to include the broadband signal effects by summing the single frequency ASFs in Equation (4) for all frequencies in the signal and taper the ASFs with the frequency spectrum. The broadband ASF is given as

$$W_{tot,BW}(k_x) = \int_{f_0}^{f_1} \mathcal{F}(f) W_{tot}(k_x(f))\, df, \tag{6}$$

where $\mathcal{F}(f)$ is the transmit waveform frequency spectrum. f_0 is the lowest and f_1 is the highest frequency of the signal. We include tapering of the LFM pulse by tapering the frequency spectrum with a Hamming taper and a Tukey taper with a cosine factor of 0.1. The receiver array weights w_n are assumed to be uniformly weighted and the transmitter weights w_m are assumed to be Hamming weights[11].

In Figure 3, we compare the ASF model to the PE grating lobes from a point scatterer simulation as a function of $u = \sin\theta$. In this dataset, the yaw error was 0.41°, the number of transmits was 53, and the number of receivers was 28. The figure shows that the ASF matches the true PE grating lobes well.

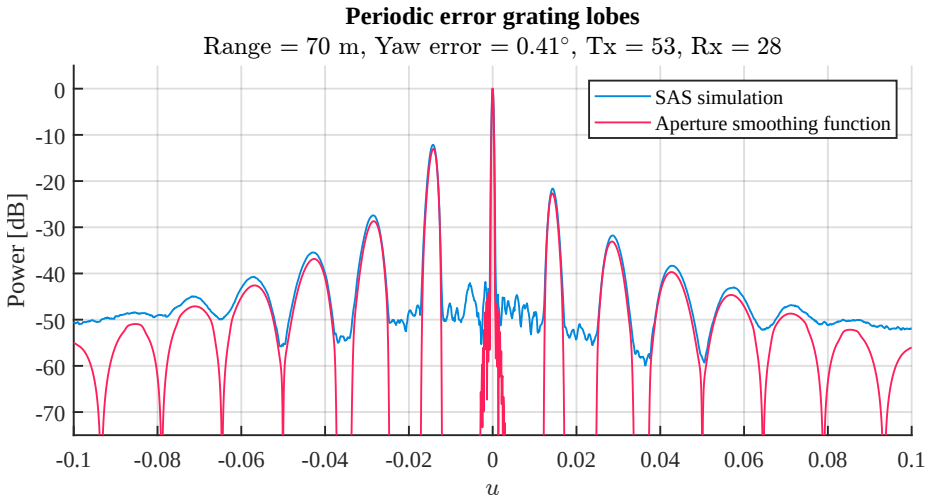

Figure 3: Broadband ASF superposed on point scatterer data at range 50 ***m with a yaw error*** $0.41°$***. The frequency spectrum and pulse are tapered. Retrieved from[8].***

The bandwidth makes the PE grating lobes wider in the along track direction and more attenuated. This is because the PE grating lobes for different frequencies appear at different angles. The width of the PE grating lobes are defined by the longest and shortest wavelength of the signal and is a function of the respective PE grating lobes' u angle. The attenuation happens because the PE grating lobes for different frequencies do not align.

The PE grating lobes are also smeared in the across track direction by uL_{VA}, where L_{VA} is the virtual array[2] length used to image a point at range y. The spread happens because the range resolution is short relative to the array extent. This causes path length differences and less overlap of pulses in the PE grating lobe directions[10]. An approximate requirement for this effect to appear is that $\Delta r < L_{VA}$ where Δr is the range resolution. When the range resolution is large relative to the array extent, $\Delta r > L_{VA}$, the range spread is given by the range resolution Δr. However, the PE grating lobe spread is never equal to Δr in SAS because of the large bandwidth and large virtual array. Thus, the PE grating lobes will always have a spread in the across track direction larger than the range resolution. Since the virtual array length increases as a function of range, this effect is more visible for larger ranges.

The smearing in the across track and along track direction causes the PE grating lobes to become trapezoidal. We verified this in the point scatterer simulations in Figure 4. The PE grating lobes do not fill the trapezoid boxes because we tapered the pulse. For untapered pulses, the PE grating lobes fill the trapezoids. Thus, the trapezoids describe the worst-case spread of the PE grating lobes.

The near field effect does not affect the PE grating lobes, since the ASF is derived based on far-field operation and agrees well with the point scatterer simulations. The reason why the near field effect is negligible may be that the PE grating lobes' u angle is small. For large u angles, the relative time delay differences over the array varies more, especially in the array's near field[10]. The relative time differences can cause additional attenuation and curving of grating lobes.

We have observed that a non-zero average yaw rotates the PE grating lobes in the images by the same angle as the yaw. This is because the transmit beam does not point perpendicular to the sonar's track. In our study, we have not included average yaw in the ASF but it can easily be included by rotating it accordingly.

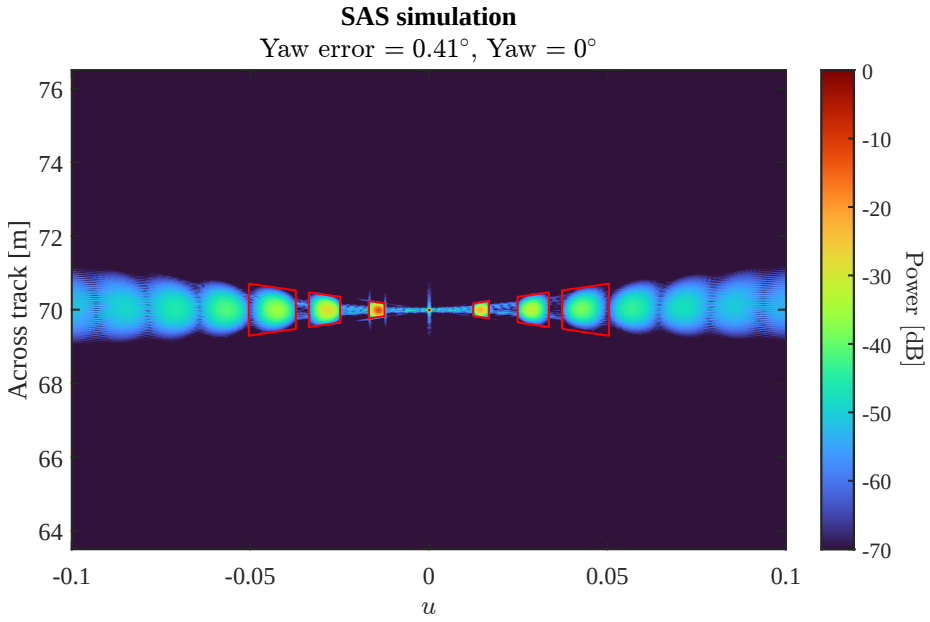

Figure 4: Trapezoids superposed on point scatterer dataset with a yaw error of $0.41°$ ***and no yaw. The trapezoids are defined by the analytical range spread, bandwidth spread, and position of the PE grating lobes.***

The datasets in Figures 3 and 4 do not have any overlap in the virtual elements, which is needed for the micronavigation of the SAS system[1]. When we included the virtual element overlap, the PE grating lobes at larger angles were reduced. This indicates that the averaging over virtual elements can reduce the PE grating lobes. The reason for this may be that the averaging over the overlapping elements reduces the periodic errors in the virtual array that we have not included in the ASF. With overlapping virtual elements, the ASF only matched the strongest PE grating lobes.

3 RESULTS

Figure 5 shows an example SAS image collected by a HUGIN AUV carrying a HISAS interferometric SAS outside Larvik, Norway, in April 2011. The scene is relatively flat and homogeneous. The image size is $240\,\text{m} \times 130\,\text{m}$ and the theoretical resolution is approximately $3\,\text{cm} \times 3\,\text{cm}$. The image is made using a delay-and-sum algorithm onto an estimated ground plane. The altitude was 20.1 m and the displacement between pings was 0.525 m. The average yaw was $0°$ during data collection. Realistic PE grating lobes in the image are created by inducing a yaw error of $0.35°$ in the delay-and-sum algorithm during imaging[5].

We created a filter from the ASF model and convolved it with error-free data to replicate true PE grating lobe distortions in Figure 5. The filter length was chosen so that it covered at least four of the largest PE grating lobes, then we convolved it along track for each across track sample.

By visual inspection it looks like the filtered output has many similarities to the dataset with realistic yaw errors in Figure 5. The strongest scatterers have defocused replicas on each side, and the position and spread of the them are approximately equal in both images. For example, the small scatterer at around $(x, y) = (56.2\,\text{m}, 92.3\,\text{m})$ in the sand is almost equally degraded in the filtered output and in the data with true yaw error (Figure 6). In addition, the areas with no strong scatterers, like in the sand, are

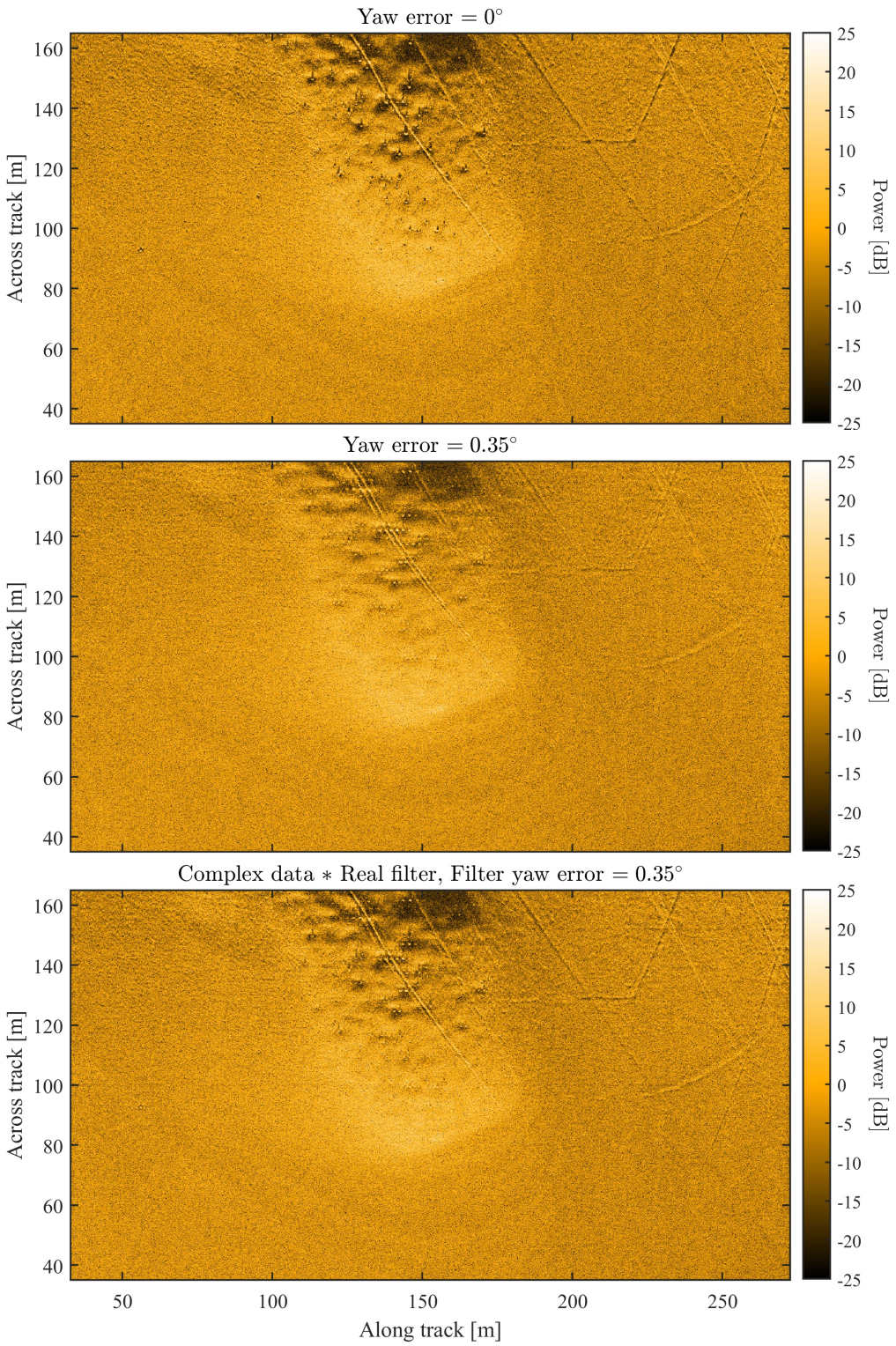

Figure 5: Example of real data SAS image. Upper panel: Without yaw error. Middle panel: With $0.35°$ ***yaw error. Lower panel: Without yaw error convolved with the ASF filter. The filter's yaw error is*** $0.35°$***. Retrieved from[8].***

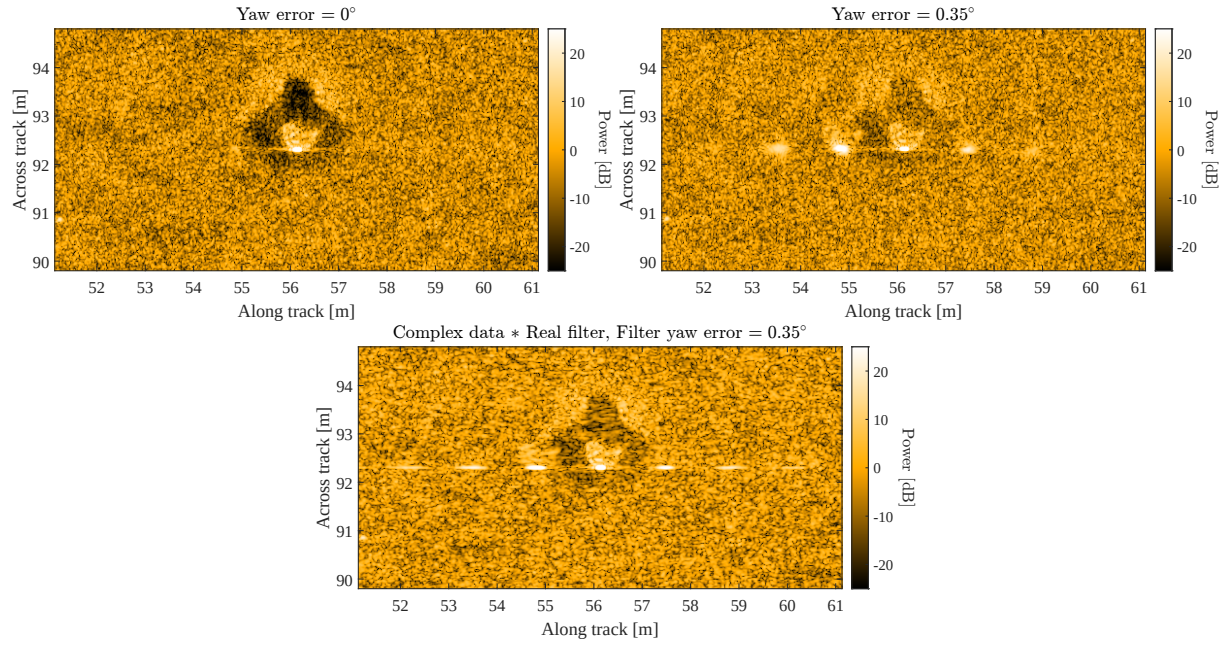

Figure 6: Zoom of region about $(x, y) = (56.2\,\boldsymbol{m}, 92.3\,\boldsymbol{m})$ ***in Figure 5.***

approximately equal. However, the one-dimensional filter does not include the spread in the across track direction due to path length differences, as shown in Figure 4. Therefore, the PE grating lobes appear smaller in the filtered output. This effect is also clearly seen in the PE grating lobes in real data in Figure 6. The shadows in the data with yaw error also appear lighter, which could be because of range spread.

In more complicated datasets where the yaw is not $0°$, the ASF can not model the PE grating lobes perfectly since the PE grating lobes are no longer aligned horizontally. This can be included by rotating the ASF filter accordingly.

4 CONCLUSION

SAS images can be degraded by defocused replicas of real targets on the seabed because of time delay errors in the beamformer. Time delay errors can occur because of navigation errors in pitch or yaw. In this paper, we have established a model based on the Aperture Smoothing Function (ASF) from array signal processing to describe the degradation due to navigation errors. The degradations appear as unequally weighted grating lobes in the ASF, which we call periodic error (PE) grating lobes. The model describes the position, amplitude, and spread of the periodic error grating lobes in point scatterer data. When filtering real data with the ASF, the degradations created from the filter resemble true degradations in real data. This opens up for new possibilities. For example, to estimate and potentially remove the errors by applying deconvolution with the filter. However, the filter should be extended to a two-dimensional filter to include two-dimensional effects such as the range spread and yaw.

REFERENCES

1. R.E. Hansen, ”Introduction to Synthetic Aperture Sonar”, in: *Sonar Systems*, N.Z. Kolev, Ed. InTech, (2011). [Online]. Available: intechopen.com
2. M.A. Richards, ”Virtual Arrays, Part 1: Phase Centers and Virtual Elements”, Georgia Institute of Technology, (2019). [Online]. Available: radarsp.weebly.com
3. R.E. Hansen, H.J. Callow, T.O. Sæbø, and S.A.V. Synnes, ”Challenges in Seafloor Imaging and Mapping With Synthetic Aperture Sonar”, *IEEE Trans. Geosci. Remote Sensing*. **49**(10) 3677–3687. (2011).
4. C.V. Jakowatz, D.E. Wahl, P.H. Eichel, D.C. Ghiglia, and P.A. Thompson, *Spotlight-Mode Synthetic Aperture Radar: A Signal Processing Approach*, Kluwer Academic Publishers, Boston, (1996).
5. M. Geilhufe, R.E. Hansen, O. Midtgaard, and S.A.V. Synnes, ”Through-the-sensor sharpness estimation for synthetic aperture sonar images”, *OCEANS 2019 MTS/IEEE SEATTLE*, 1-6. Seattle (2019).
6. D.H. Johnson and D.E. Dudgeon, *Array Signal Processing: Concepts and Techniques*, PTR Prentice Hall, (1993).
7. T.O. Sæbø, ”Seafloor depth estimation by means of interferometric synthetic aperture sonar”, Doctoral thesis, The Arctic University of Norway. (2010). [Online]. Available: munin.uit.no
8. M. Opperud, ”Grating lobe errors in synthetic aperture sonar images”, Master thesis, University of Oslo. (In prep.). [Online]. Available: duo.uio.no
9. D.A. Cook, and D.C. Brown, ”Analysis of Phase Error Effects on Stripmap SAS”, *IEEE J. Oceanic Eng.* **34**(3) 250-261. (2009).
10. B.A.J. Angelsen, *Ultrasound Imaging: Waves, Signals, and Signal Processing*, Emantec, (2000).
11. F.J. Harris, ”On the use of windows for harmonic analysis with the discrete Fourier transform”, *Proceedings of the IEEE*, **66**(1) 51-83. (1978).